Separation of superparamagnetic particles through ratcheted Brownian motion and periodically switching magnetic fields

Fan Liu,[1] Li Jiang,[2] Huei Ming Tan,[3] Ashutosh Yadav,[1] Preetika Biswas,[1] Johan R. C. van der Maarel,[1] Christian A. Nijhuis,[2] and Jeroen A. van Kan[1,a)]
[1]*Department of Physics, National University of Singapore, Singapore 117542*
[2]*Department of Chemistry, National University of Singapore, Singapore 117543*
[3]*Engineering Science Programme, National University of Singapore, Singapore 117576*

(Received 25 August 2016; accepted 4 November 2016; published online 15 November 2016)

Brownian ratchet based particle separation systems for application in lab on chip devices have drawn interest and are subject to ongoing theoretical and experimental investigations. We demonstrate a compact microfluidic particle separation chip, which implements an extended on-off Brownian ratchet scheme that actively separates and sorts particles using periodically switching magnetic fields, asymmetric sawtooth channel sidewalls, and Brownian motion. The microfluidic chip was made with Polydimethylsiloxane (PDMS) soft lithography of SU-8 molds, which in turn was fabricated using Proton Beam Writing. After bonding of the PDMS chip to a glass substrate through surface activation by oxygen plasma treatment, embedded electromagnets were cofabricated by the injection of InSn metal into electrode channels. This fabrication process enables rapid production of high resolution and high aspect ratio features, which results in parallel electrodes accurately aligned with respect to the separation channel. The PDMS devices were tested with mixtures of 1.51 μm, 2.47 μm, and 2.60 μm superparamagnetic particles suspended in water. Experimental results show that the current device design has potential for separating particles with a size difference around 130 nm. Based on the promising results, we will be working towards extending this design for the separation of cells or biomolecules. *Published by AIP Publishing.* [http://dx.doi.org/10.1063/1.4967965]

INTRODUCTION

To realize the vision of the lab-on-a-chip (LOC) platform as a viable and practical technology, a diverse range of subsystems of various functionalities need to be developed, miniaturized, and integrated into a complete system. In this regard, the ability to quickly and accurately sort particles within a compact footprint is a vital component of a LOC. Combined with a relatively low cost fabrication, the resultant massive parallelization can be leveraged to enable high-throughput sorting.

In general, techniques for particle separation and sorting are categorized into active and passive techniques or a combination of the two.[1] In the category of active techniques, forces generated from acoustic waves, electric or magnetic fields, and optical tweezers are used to sort particles.[2,3] For techniques employing magnetic fields, in particular, relatively large external permanent magnets are usually used to create magnetic forces acting on the particles in separation channels.[4,5] While all types of particle separation and sorting techniques are effective in their respective performance regimes, not all techniques have a compact footprint, especially for the sorting of submicron particles due to reduced sorting efficiency caused by Brownian motion of particles.

In this paper, we demonstrate a novel active particle separation and sorting technique which harnesses periodically switching magnetic fields and Brownian motion. This technique is

a)Author to whom correspondence should be addressed. Electronic mail: phyjavk@nus.edu.sg

implemented in a compact microfluidic chip with asymmetric sawtooth sidewalls in the separation channel. The microfluidic particle separators are obtained through Polydimethylsiloxane (PDMS) soft lithography of SU-8 molds, fabricated with proton beam writing (PBW).[6,7] After oxygen plasma treatment to enable the PDMS chip to bond to a glass substrate, the cofabrication of electromagnet channels[8] completes the device fabrication process. This work represents an extension of previous experiments employing gravity[9] which validated the applicability of a theoretical model for a Brownian ratchet with improved characteristics for particle separation.[10]

Subsequent sections of this paper provides a brief overview of particle sorting with Brownian ratchets; the fabrication strategy and methods used in creating the microfluidic device; experimental setup and testing with mixed pairs of $2.60 \pm 0.13\,\mu$m, $2.47 \pm 0.07\,\mu$m, and $1.51 \pm 0.05\,\mu$m magnetic particles suspended in water; the results and discussion of the achieved sorting performance as well as its applicability to potential applications.

Preamble to Brownian ratchets in microfluidics

Any particle suspended in a liquid media experiences Brownian motion, a phenomenon whereby the particle is constantly jostling with and jostled by other particles or fluid molecules in the fluid due to their inherent thermal energy. As a result, the suspended particle trajectories adopt a random walk, with smaller particles exhibiting greater Brownian motion at a given temperature and fluid viscosity. At thermal equilibrium, the Brownian motion generated by thermal noise is symmetric, even in an anisotropic medium. In Feynman's conceptual discussion of a microscopic ratchet and pawl model which rectifies the movement of gas molecules between two compartments, a system at thermal equilibrium is unable to harness Brownian motion alone to sort particles.[11]

However, in a system driven out of equilibrium through the introduction of a periodic potential field (which would exert drift forces on particles) and symmetry breaking, rectified particle motion is indeed possible as initially demonstrated by Rousselet *et al.*[12] Symmetry breaking can be achieved through a combination of the following: asymmetrical physical features, i.e., Deterministic Lateral Displacement (DLD),[13,14] modulation of the potential or dynamics that break the symmetry in the time domain. The reader is directed to Refs. 15 and 16 for a general discussion of Brownian ratcheting schemes. Brownian ratchet separation techniques have some advantages over traditional separation methods such as gel electrophoresis, among them the capability for continuous separation.

The extended on-off Brownian ratchet

Classical implementations of DLD sieves have two disadvantages, requiring localized injection of particles for operation and the dependence of separation resolution on obstacle array size. For example, a sorting array roughly $\sim 3 \times 10\,\text{mm}^2$ was used by Huang *et al.*[17] Nevertheless, it is thought that direction reversal, whereby the directionality of particle flow can be inverted by adjusting system parameters can overcome both disadvantages.

In a simple on-off ratchet, an asymmetric sawtooth potential is periodically switched on and off to induce particle drift. Over time, the particles will exhibit rectified average displacement. Grimm *et al.*[10] proposed an extended on-off ratchet model which allows for direction reversal. In this extended model, a second asymmetric sawtooth potential is included which has equal but inverse magnitude and double the periodicity to the first potential. The interplay of particle drift arising from the potentials applied and the Brownian motion experienced by the particle causes rectified average displacement of the particles. By controlling system parameters such as the cycle time to modulate between the two potentials, such a device has the selectivity and flexibility to control average displacement of two different particle populations.

Subsequently, the applicability of the ratchet configuration in microfluidics was demonstrated by Verleger *et al.* in the fabrication and characterization of a compact microfluidic single-channel Brownian ratchet with a channel footprint of roughly $0.1\,\text{mm}^2$.[9] The extended on-off ratchet was implemented through the fabrication of a microfluidic channel with asymmetric sawtooth sidewalls and using gravity as the driving force. Through the use of gravity to

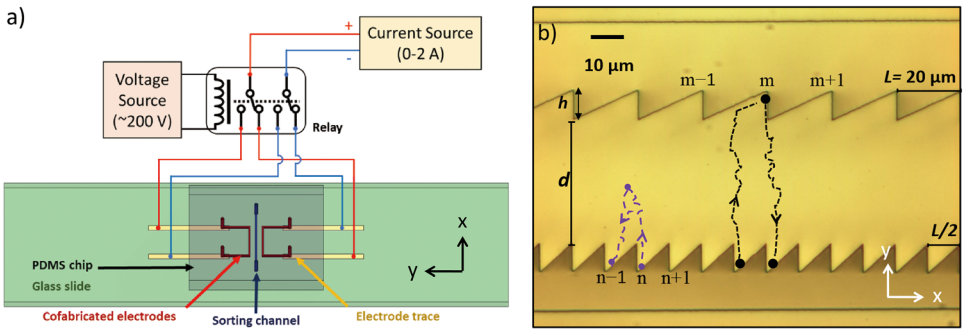

FIG. 1. (a) Schematic representation of separating device and apparatus for generating magnetic fields in the microfluidic chip. (b) Annotated image of separation channel of width d, sawtooth length L, and sawtooth height h in fabricated chip, illustrating a full cycle of separation. The borders of cofabricated electrode channels are partially visible at the top and bottom of image.

exert a force on the particles in the microfluidic channel, the particles drifts back and forth between the sawtooth sidewalls on both sides of the channel. Subsequently, the average displacement of particles along the channel is rectified as predicted in the extended on-off Brownian ratchet model.[10] In this configuration, separation of 3.0 μm and 4.3 μm silica microparticles suspended in water was demonstrated and the magnitude of average displacement of two different particle sizes can be changed by modulating the duration of the drift force applied.

As gravity is an impractical approach to apply drift forces on suspended particles, we present another implementation of the extended on-off ratchet model in microfluidics using magnetic fields. The magnetic field is generated through alternating and cyclical application of current flowing through a pair of metal electrodes, parallel to a microfluidic separation channel with asymmetric sawtoothed sidewalls (Fig. 1(a)). The magnetic field generated induces drift of magnetically susceptible particles in the separation channel, causing the particles to cycle back and forth in the channel's y-axis, as the particle simultaneously experiences Brownian motion. As particles arrive at either side of the sawtooth sidewalls, they are laterally displaced along the x-axis as they slide along the sawtooth sidewall profiles. For particle separation to occur in the sorting channel, particles in the channel must experience different drift velocities arising from the magnetic field generated by the currents in the electromagnets. Additionally, the cycle of alternating direction of induced magnetic drift needs to be chosen such that (Fig. 1(b)) the particle with slower drift velocity (purple) interacts only with the bottom sawtooth profile, whereas the particle with faster drift velocity (black) interacts with both sawtooth profiles. Over multiple cycles, the slower particles will develop a negative average displacement along the x-axis and the faster particles will develop a positive average displacement along the x-axis. Figure 2 shows the magnetic force experienced by particles and current pattern through the electrodes. In our experiment, the magnetic particles are driven by magnetic fields in the y direction, and therefore, the effective drift in y is a combination of Brownian motion, magnetic

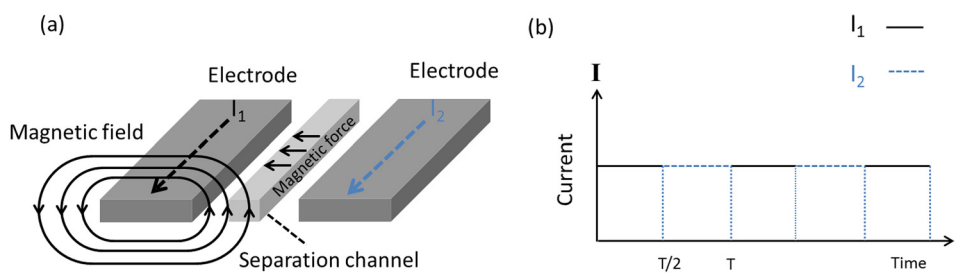

FIG. 2. (a) Illustration of the introduction of alternating magnetic fields generated by electrodes functioning as electromagnets and resultant force created in the separation channel; (b) current waveforms showing how the currents (I_1 and I_2) were switched on and off periodically to flip the resulting magnetic force in the separation channel, and T is the cycle time.

drift force, and Stokes drag. In the x direction, the particles will diffuse freely once free of the sawtooth profile and therefore its behavior is purely Brownian. These conditions allow us to decouple the particle movement in x and y directions. To calculate the probability distribution of a particle under Brownian motion in the x-axis, we start with the Stokes-Einstein equation

$$\frac{\partial P(x, t_{\text{diff}})}{\partial t} = D \frac{\partial^2}{\partial x^2} P(x, t_{diff}), \tag{1}$$

where D and t_{diff} represent the diffusion coefficient and diffusion time, respectively. The solution for this equation is

$$P(x, t_{\text{diff}}) = \frac{1}{\sqrt{4\pi D \text{t}_{\text{diff}}}} \exp\left(-\frac{x^2}{4D t_{\text{diff}}}\right), \tag{2}$$

showing that probability distribution P of a particle at time t_{diff} has a Gaussian distribution. For example, the probability for a particle to diffuse from position n to n–1 in Fig. 1(b) can be estimated through the integration of the probability distribution

$$P = \int_n^{n-1} P(x, t_{\text{diff}}) dx. \tag{3}$$

Here, n is the small sawtooth position and t_{diff} the diffusion time for a particle. The reader is directed to Ref. 10 for a more detailed treatment of the extended on-off ratchet model. The displacement for the particle is a multiple of L/2 and the average displacement per cycle can be theoretically estimated to be $P\left(\frac{L}{2}\right)$, for optimized diffusion time.

EXPERIMENTAL

Fabrication approach and design

In order to have a compact and integrated microfluidic design with switchable magnetic fields aligned with the separation channel, co-fabrication[6] was used to incorporate metal electrodes into the device to serve as electromagnets. To obtain relatively high magnetic field gradients, the electromagnet electrodes should be as close as possible to the separation channel. Additionally, the cross section of the co-fabricated electromagnet channels should be as large as possible to facilitate metal solder injection and operate with relatively high currents. As such, this requires the separation channel to have a high aspect ratio to facilitate ease of fabrication. This has the added benefit of the separation channel having a larger sorting volume resulting in increased throughput. Furthermore, the separation channel sidewalls should be as smooth as possible so not to trap or hinder the motion of the particles we intend to separate. Given the need for both high resolution and aspect ratio fabrication, direct PBW is chosen over conventional lithographic techniques to fabricate the separation channel. This is due to the fact that MeV proton beams maintain practically straight trajectories with deep penetrating range, which allows for the fabrication of 3D, high aspect ratio structures with vertical, smooth sidewalls and low line-edge roughness.[18] In addition, when PBW is used in conjunction with imprinting or soft lithography, chip fabrication speeds can be vastly increased with the duplication of master molds for multiple usage.

In our design, a 27 μm thick and 320 μm long separation channel with sawtooth sidewalls was fabricated with the following dimensions: width d = 40 μm; sawtooth length, L = 20 μm; and sawtooth height, h = 10 μm. This yields an aspect ratio of over 50 based on the sawtooth edges having a measured size of around 500 nm for the 27 μm thick separation channel. The separation channel is bracketed by two equally thick electromagnet channels 100 μm wide, running in parallel. The two electromagnet channels have a center to center gap distance of 180 μm, and can handle currents up to 0.6 A (giving a magnetic field of $\sim$1 mT).

Proton beam writing with SU-8 photoresist and PDMS casting

A Si wafer (Silicon, Inc.) was dehydrated by baking on a hot plate at 150 °C for 10 min. After that, a 27 μm thick MicroChem SU-8 2025 photoresist was spin coated on to the wafer at 3000 rpm coating speed for 30 s, following by soft baked first at 65 °C for 3 min and 95 °C for 5 min. For PBW, a 2 MeV proton beam approximately 200 nm (x-axis) by 300 nm (y-axis) spot size was used to fabricate a separation channel with asymmetric sawtooth sidewalls in the SU-8 photoresist, within a scan area of 320 μm × 320 μm using an algorithm for magnetic beam scanning.[19] This was followed by a stage translation plus beam scanning algorithm[20] to fabricate two 50 μm wide feeding channels and 100 μm electrode channels beside the separation channels. When the PBW process is completed, the features in the SU-8 master mold were developed by immersion in pure SU-8 developer for 5 min, then washed with isopropanol (IPA) and the fabricated features are characterized with a Scanning Electron Microscope (Fig. 3(a)).

Casting high aspect ratio PDMS structures by soft lithography[21] is challenging due to the low Young's modulus of PDMS which makes it difficult to successfully demold the structures.[22,23] Therefore, a solution of 0.04% Teflon AF 1600 (DuPont Fluoroproducts) diluted in FC-40 (Acros Organics) was spin coated onto the SU-8 master mold at a speed of 1500 rpm and baked at 120 °C for 12 h.[24] Besides allowing for easy demolding, this fluorinated layer also serves as a protective coating for the master mold.[25] Then, PDMS soft lithography was done using the completed SU-8 masters. Finally, 1 mm diameter holes were punched into the PDMS chip to facilitate fluid injection into the separation channel.

Sputtering of electrode traces on glass and PDMS bonding

To facilitate the electrical connection between the electrode channels and current power supply, a magnetron sputtering machine and a stencil mask made of Kapton foil were used for stencil deposition of chrome, and then gold onto glass slides. Then, the PDMS chips are bonded to the glass slides by oxygen plasma treatment (Harrick Plasma) using 300 mTorr ambient air at 18 W for 30 s. As the sputtered electrode traces are of millimeter dimensions, the PDMS chip and glass slide can be aligned by eye for bonding.

Co-fabrication of electromagnet metal channels

The co-fabrication process used has been outlined in Ref. 26. A solution of 0.1 M 3-mercaptopropyltrimethoxysilane in acetonitrile was first injected into the electrode channels and left to dry at room temperature. This solution is injected to help ensure continuous filing of

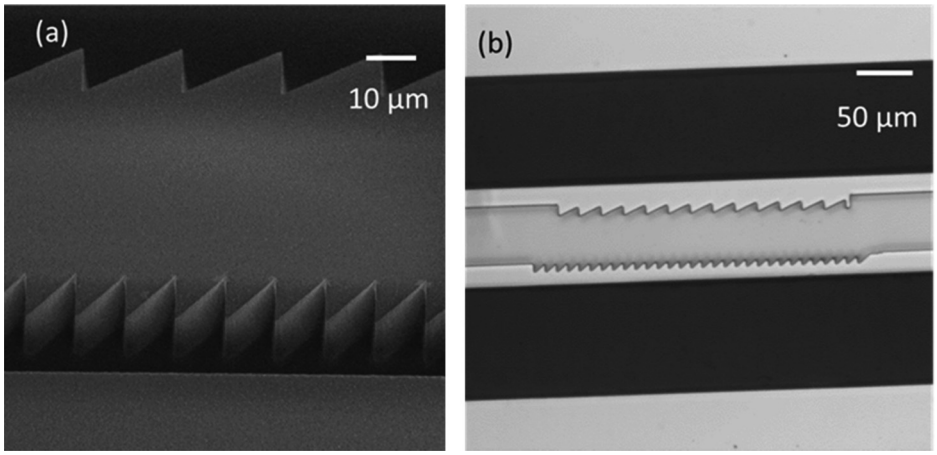

FIG. 3. (a) A Scanning Electron Microscope (SEM) image of a 27 μm tall SU-8 ratchet mold fabricated with PBW. (b) Optical image of PDMS ratchet channel and electromagnet channels filled with InSn.

the channel with InSn during the subsequent injection step. To prepare the solder material for injection, a slab of 52% Indium and 48% Tin solder (The Indium Corporation of America) was placed on the top of the electrode channels inlet and melted by baking in an oven for 15 min at 130 °C. Then, a pre-heated Micro-Mate 20 cc glass syringe (Cadence Science) was used to inject the liquid InSn solder into the channels. The finished device was then characterized by optical microscopy (Fig. 3(b)).

Device operation and experimental setup

The experimental setup (Fig. 1(a)) consists of the fabricated device wired to a Type 6012 relay, which in turn is connected to a 2 A current power supply and a 220 V high voltage (HV) amplifier. The HV amplifier is computer controlled with a LabVIEW (National Instruments) Virtual Instrument and an NI 9263 Analog Output module, which provides a control voltage signal to the HV amplifier unit. In this configuration, a 200 V switching voltage is provided to the relay, therefore modulating the switching of current from one electrode to another. The sorting device was mounted on an inverted microscope (Olympus IX-71), imaging was done with an Evolve 512 EMCCD camera (Photometrics), and the captured images are processed with ImageJ (US NIH).

For the sorting experiments, 2.60 μm COMPEL (Bangs Laboratories, 5% coefficient variation) polymer beads as well as 1.51 μm and 2.47 μm MAG silica (Microparticles GmBH, 3.3% and 2.9% coefficient variation, respectively) superparamagnetic particles were selected.

Superparamagnetic particles excel for this purpose as they have no magnetic memory and have nano-sized iron oxide (magnetite) uniformly dispersed in the polymer/silica matrix. Additionally, these particles can be modified with carboxyl groups and therefore can be bound to biomolecules (e.g., cells and DNA) for further studies and applications.

RESULTS AND DISCUSSION

In the initial set of experiments, a homogeneous mixture of two superparamagnetic particles suspended in water was introduced into the separation channel and flow velocities in the channel were nulled before starting of the experiments. Currents up to 0.5 A were then applied to the electromagnets, with cycle times of 50–83 s. The magnetic drift force was flipped at the midpoint of each cycle. Particles with less magnetic susceptibility will only interact with the small sawtooth sidewalls and develop a negative average displacement along the x-axis. In the meantime, the particles with a larger magnetic susceptibility experiences higher drift and thus interact with the sawtooth sidewalls on both sides of the channel. In the experiments, the displacement in the x-axis was measured after each cycle. The average displacement (AD) based on measured values from the experiments is then

$$\mathrm{AD} = \mathrm{X}/\mathrm{N}, \tag{4}$$

where X is the total displacement and N is the total number of events of the particles during an experiment.

As average displacement is affected by the choice of cycle time and electrode current used, five experimental sessions were conducted with different cycle time and current (Fig. 4(a)). The cycle time was chosen such that particles with the smaller magnetic susceptibility interact only with the smaller sawtooth profile and particles with larger magnetic susceptibility will interact with both sawtooth profiles. For example, in Experiment 2, the cycle time T = 63 s was used, as the average diffusion time for 1.51 μm (purple) and 2.60 μm (black) particles was measured to be around 25 s and 20 s, respectively. In Fig. 5, the probability density distributions for a representative 1.51 μm and 2.60 μm particle was calculated with Eq. (2) for time t = 11 s, 32 s, and 43 s and graphed. At t = 32 s, the probability for a 2.60 μm particle was also calculated using Eq. (3) and graphed. Thus, Fig. 5 illustrates that both particle populations will exhibit direction reversal and move in two opposite directions in the channel over successive cycles.

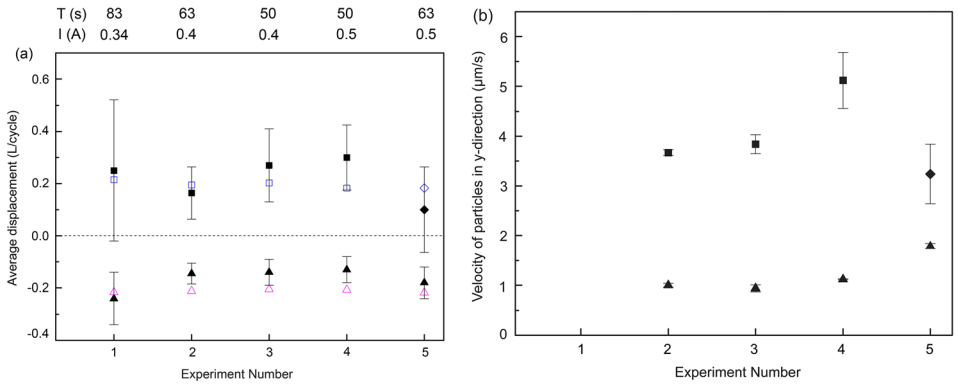

FIG. 4. Five groups of experiments were conducted with different cycle time and current. The sizes of the particles are 2.60 μm (box), 2.47 μm (diamond), and 1.51 μm (upper triangle). Closed symbols are experimentally measured values, and open symbols are calculated values (using Eq. (3)). (a) Average displacement scaled to period length (L = 20 μm) per cycle from each experimental session (1–5, using cycle times T and currents I listed at top of graph), within 90% confidence range. (b) Average particle velocities in the y-direction from each experimental session (1–5), within 90% confidence range.

For the results in Fig. 4, the calculated values for the 1.51 μm and 2.60 μm particle populations are close and within the estimated confidence range of the measured values. However, there is a small mismatch for the smaller 1.51 μm particle population (in Experiments 2, 3, and 4). This mismatch can be explained due to the attractive behavior of the smaller

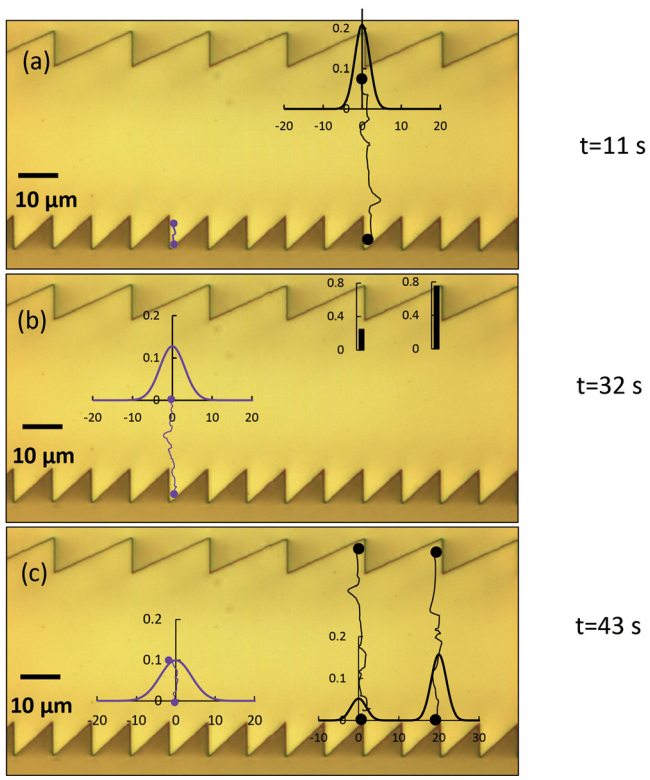

FIG. 5. Illustration of two different size particle movement at certain time t with cycle T of 63 s. (a) Position of particles at t = 11 s, with dashed line showing traveled trajectory from t = 0 s. The Gaussian distributions represent the probability density distribution of particles. (b) Particles at t = 32 s, with the black particle at minima of big sawtooth profile. The black bars represent the probability at those two sites according to Eq. (3); the purple particle respond to the magnetic field with a Gaussian distribution. (c) Particle positions at t = 43 s, with dashed line indicating trajectories traveled from t = 32 s, with their respective probability density distributions shown.

superparamagnetic particles with the small sawtooth sidewalls. During the separation cycle, particles are expected to drift to a sawtooth minimum under the influence magnetic fields. Upon the reversal of the direction of magnetic force, the particle is expected to immediately drift towards the opposite channel sidewall. Instead, in the experiments, it has been observed that the smaller particles tend to slide along the sawtooth profiles (possibly due to attractive van der Waals forces) for some distance before detaching from the wall, therefore resulting in a positive offset in average displacement (Fig. 6). This response is not readily apparent in the behavior of the larger particles, likely due to the larger magnetic drift force induced compared to the attractive van der Waals forces to the channel sidewalls.

In this single channel ratchet design, the key variable for particle separation are the particles' y-axis drift velocities which in turn affects design considerations and operating parameters. The average velocity of particles for Experiments 2 to 5 were measured and graphed in Figure 4(b). With a current of 0.4 A in Experiments 2 and 3, the 2.60 μm polymer particles had an average velocity of 3.75 ± 0.16 μm/s. When the current was increased to 0.5 A in Experiment 4, the average velocity of the 2.60 μm polymer particles increased to 5.12 ± 0.55 μm/s. Similarly, average velocities for 1.51 μm silica particles are 0.98 ± 0.02 μm/s (for Experiments 2 and 3) and 1.12 ± 0.05 μm/s for Experiment 4.

A comparison between Experiments 4 and 5 revealed that the 1.51 μm silica particles in Experiment 5 have a higher average drift velocity (1.7 ± 0.05 μm/s). This was due to the use of a modified design in Experiment 5, having a smaller channel width, d and electromagnets closer to the separation channel which resulted in a higher magnetic drift force for the same current applied. In addition, the 2.47 μm silica particles in Experiment 5 have a slower average drift velocity (3.24 ± 0.60 μm/s) than the 2.60 μm polymer particles (5.12 ± 0.55 μm/s) in Experiment 4. Despite the larger magnetic force, the 2.47 μm silica particles still drifted slower than 2.60 μm polymer particles. This was attributed to the different densities for the two particle materials ($\sim$2.0 g/cm^3 for silica and $\sim$1.2 g/cm^3 for polymer) and magnetite concentration which would affect the drift force experienced by the particles. As such, it is possible to achieve particle separation with a size difference of only 130 nm.

We also considered the influence of fluid flow on the separation performance of our device by connecting MFCS microfluidic flow control (Fluigent) to the separation channel reservoirs (Fig. 7). In Experiment 6, fluid flow was tuned to null the average displacement of the smaller 1.51 μm silica particles. The larger 2.60 μm polymer particles then achieved a larger average displacement (0.7 l/cycle) compared to previous separation experiments, validated by microscope observations (Fig. 8). In Experiment 7, the fluid flow was reversed and the average displacement for the larger 2.60 μm polymer particles was nulled. The corresponding average

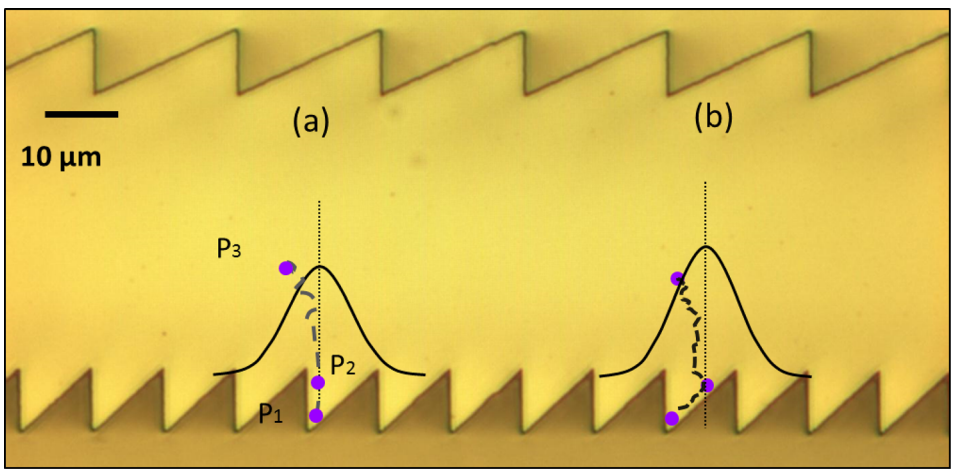

FIG. 6. (a) Gaussian distribution of Brownian particle. (b) Particle sliding along the ratchet after change of field direction, leading to shorter diffusion time.

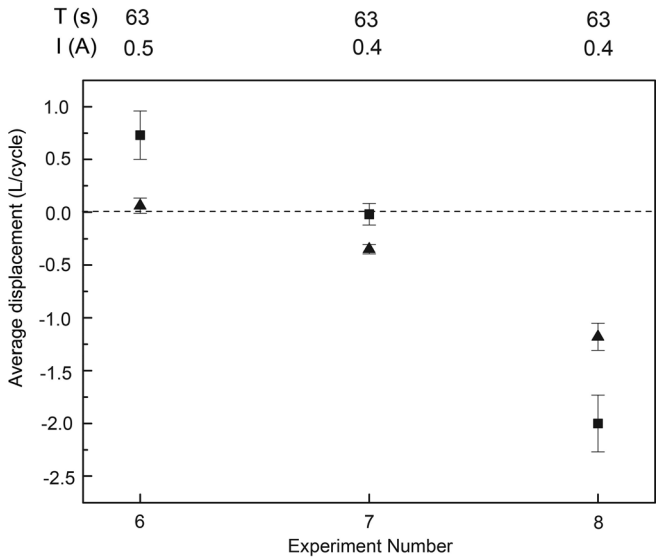

FIG. 7. Average displacement in periodicity L (20 μm) per cycle versus experiment number with a net flow in the channel, the sizes of the particles are 2.60 μm (box), and 1.51 μm (upper triangle); Estimated confidence range represents 90% of the experimental results.

displacement for the 1.51 μm silica particles is 0.4 l/cycle. Last, in Experiment 8 a larger flow velocity is applied and although the average displacement for both the 1.51 μm silica particles and 2.60 μm polymer particles are measured to be negative, both average displacements are still rectified.

CONCLUSION

Based on our recorded observations, we can conclude that the current device design has the resolution for separating particles with a size difference of 130 nm, and with some adjustments the separation resolution can be further refined. Additionally, particle separation in our device is relatively independent from fluid flow along the separation channel (x-axis) and also had the added benefit of demonstrating selective particle separation.

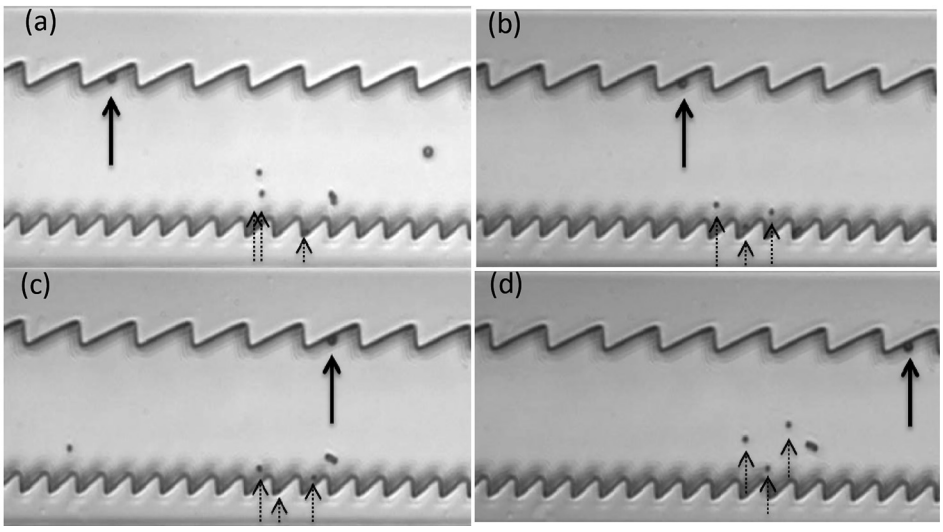

FIG. 8. Screen capture with microscope camera showing selective displacement 2.60 μm polymer particles with null average displacement of 1.51 μm silica particles over ten cycles in Experiment 6: (a) 1st cycle, (b) 5th cycle, (c) 7th cycle, and (d) 10th cycle.

A comparison with the previously demonstrated gravity based particle separator shows that using a magnetic Brownian separator is around 10 times faster due to the smaller channel dimension and high aspect ratio as well as larger Brownian motion. This also allows separation of smaller particles down to one micron. With further miniaturization of chip dimensions (at least threefold), separation of smaller magnetic particles is potentially realizable. The separation time can be further reduced to 20 min according to an estimation with reduced length scales.[9] Therefore, our implementation of the extended on-off Brownian ratchet model using magnetic fields enables the separation of magnetically susceptible particles or molecules, such as magnetically labelled cells, which are frequently used in clinical research and applications.

Based on the promising results, we will be working towards extending this design for cell or biomolecule separation (e.g., DNA, proteins, or cells). One approach is to attach magnetic labels to the biomolecules,[27] of which the magnetic particles for binding are already widely available from different companies such as Dynal, Bangs Laboratories and Polysciences. Another approach is to use paramagnetic buffer (such as MnCl2 and Gd·DTPA), which has been demonstrated with cells (human blood cell, yeast, and algae).[28–30]

ACKNOWLEDGMENTS

We acknowledge and thank the following Singapore institutions for their funding in support of our work: the National Research Foundation (NRF), Prime Minister's Office [Competitive Research Programme (CRP) Grant No. NRF-CRP 8-2011-07], and the Ministry of Education (MOE) [Academic Research Fund (AcRF) Grant No. R-144-000-312-112]. We also acknowledge additional funding support from NRF through its Medium-Sized Centre.

[1]P. Sajeesh and A. K. Sen, Microfluid. Nanofluid. **17**, 1 (2014).
[2]B. Cetin, M. B. Ozer, E. Cagatay, and S. Buyukkocak, Biomicrofludics **10**, 014112 (2016).
[3]C. Iliescu, G. Tresset, and G. L. Xu, Biomicrofludics **3**, 044104 (2009).
[4]L. Zanini and T. Houssin, "Microfluidic Magnetic Particle Sorting and Separation: A Short Review," Elveflow, 2016; see http://www.elveflow.com/microfluidic-tutorials/microfluidic-reviews-and-tutorials/magnetic-particle-separation-a-short-review/.
[5]M. Hejazian and N.-T. Nguyen, Biomicrofludics **10**, 044103 (2016).
[6]J. A. van Kan, P. Malar, and A. B. Vera, Rev. Sci. Instrum. **83**, 02B902 (2012).
[7]Y. Yong and J. A. van Kan, Nucl. Instrum. Methods Phys. Res. B **348**, 203 (2015).
[8]A. C. Siegel, S. K. Y. Tang, C. A. Nijhuis, M. Hashimoto, S. T. Phillips, M. D. Dickey, and G. M. Whitesides, Acc. Chem. Res. **43**, 518 (2010).
[9]S. Verleger, A. Grimm, C. Kreuter, H. M. Tan, J. A. van Kan, A. Erbe, and J. R. C. van der Maarel, Lab Chip **12**, 1238 (2012).
[10]A. Grimm, H. Stark, and J. R. C. van der Maarel, Phys. Rev. E **79**, 061102 (2009).
[11]R. P. Feynman, R. B. Leighton, and M. Sands, *The Feynman Lectures on Physics* (Addison-Wesley, Reading, MA, 1966).
[12]J. Rousselet, L. Salome, A. Ajdari, and J. Prostt, Nature **370**, 446 (1994).
[13]T. A. J. Duke and R. H. Austin, Phys. Rev. Lett. **80**, 1552 (1998).
[14]C. F. Chou, O. Bakajin, S. W. P. Turner, T. A. J. Duke, S. S. Chan, E. C. Cox, H. G. Craighead, and R. H. Austin, Proc. Natl. Acad. Sci. **96**, 13762 (1999).
[15]R. D. Astumian, Science **276**, 917 (1997).
[16]P. Hänggi and F. Marchesoni, Rev. Mod. Phys. **81**, 387 (2009).
[17]L. R. Huang, E. C. Cox, R. H. Austin, and J. C. Sturm, Science **304**, 987 (2004).
[18]F. Watt, M. B. H. Breese, A. A. Bettiol, and J. A. van Kan, Mater. Today **10**, 20 (2007).
[19]A. A. Bettiol, C. N. B. Udalagama, J. A. van Kan, and F. Watt, Nucl. Instrum. Methods Phys. Res. B **231**, 400 (2005).
[20]Y. Yao, P. S. Raman, and J. A. van Kan, Microsyst. Technol. **20**, 2065 (2014).
[21]D. C. Duffy, J. C. MacDonald, O. J. A. Schueller, and G. M. Whitesides, Anal. Chem. **70**, 4974 (1998).
[22]I. D. Johnston, D. K. McCluskey, C. K. L. Tan, and M. C. Tracey, J. Micromech. Microeng. **24**, 035017 (2014).
[23]H. Shinohara, H. Goto, T. Kasahara, and J. Mizuno, Micromachines **4**, 157 (2013).
[24]C. Zhang, K. Jiang, F. Liu, P. S. Doyle, J. A. van Kan, and J. R. C. van der Maarel, Lab Chip **13**, 2821 (2013).
[25]P. G. Shao, J. A. van Kan, and F. Watt, Key Eng. Mater. **447–448**, 452 (2010).
[26]A. C. Siegel, S. S. Shevkoplyas, D. B. Weibel, D. A. Bruzewicz, A. W. Martinez, and G. M. Whitesides, Angew. Chem., Int. Ed. **45**, 6877 (2006).
[27]N. Pamme, Lab Chip **6**, 24 (2006).
[28]R. Zhou and C. Wang, Biomicrofluidics **10**, 034101 (2016)
[29]H. Watarai and M. Namba, J. Chromatogr. A **961**, 3 (2002).
[30]A. Winkleman, K. L. Gudiksen, D. Ryan, and G. M. Whitesides, Appl. Phys. Lett. **85**, 2411 (2004).